CHEMBIOCHEM

Supporting Information

Lamprey Parapinopsin ("UVLamP"): a Bistable UV-Sensitive Optogenetic Switch for Ultrafast Control of GPCR Pathways

Dennis Eickelbeck,*[a] Till Rudack,[b, c] Stefan Alexander Tennigkeit,[b, c] Tatjana Surdin,[a] Raziye Karapinar,[a] Jan-Claudius Schwitalla,[a] Brix Mücher,[a] Maiia Shulman,[b, c] Marvin Scherlo,[b, c] Philipp Althoff,[b, c] Melanie D. Mark,[a] Klaus Gerwert,*[b, c] and Stefan Herlitze[a]

cbic_201900485_sm_miscellaneous_information.pdf

Experimental procedure

Generation of plasmid constructs

To construct adeno-associated virus (AAV) expression vectors and allow for the necessary large packaging capacity, the pAAV-CW3SL-EGFP vector (GenBank accession number: KJ411916.2) was used as the backbone plasmid for all opsin constructs [1]. The Japanese lamprey parapinopsin (*Lethenteron camtschaticum*, GenBank accession number: AB116380.1, as submitted to GenBank in 2003 [2]) cDNA was inserted into the vector removing the stop-codon and adding a c-terminal eGFP as a fluorescence marker. This construct will be named parapinopsin or UVLamP in the following. Each element was PCR amplified with 16bp overhangs and inserted into the backbone via AQUA Cloning for expression under the CMV promoter [3]. The mouse melanopsin control plasmid was generated accordingly exchanging the eGFP for an mCherry fluorescence tag, as described in our previous publication [4]. The green and red Ca^{2+} sensors GCaMP6m and jRCaMP1b as well as the red cAMP indicator Pink Flamindo were used unmodified as described in their respective publications [5].

Cell culture and *in vitro* imaging

Human embryonic kidney (HEK) tsA201 cells and HEK GIRK 1/2 cells (HEK293 cells stably expressing GIRK1/2 subunits, kindly provided by Dr. A. Tinker UCL London, GB) were maintained at 37 °C in Dulbecco's modified Eagle's medium (DMEM), 4.5 g l^{-1}D-glucose, supplemented with 10% fetal bovine serum (Gibco) and penicillin/streptomycin in a humidified incubator under 5% CO_2. Growth medium of stable cell lines was supplemented with G418 (5 mg/ml). Cells were cultured on 35 mm glass bottom dishes (for imaging) or plastic bottom dishes (for electrophysiology). Cells were transfected with UVLamP or mouse melanopsin via FuGENE® HD (Promega) according to the manufacturer's protocol and incubated for 18-24 h before recordings. For opsin experiments 9-cis retinal was added to a final medium concentration of 1 µM. To image Ca^{2+} signals in HEK tsA201cells via GCaMP6m or jRCaMP1b, cells were transiently co-transfected with UVLamP + jRCaMP1b or mouse melanopsin + GCaMP6m. Cells were seeded into poly L-lysine coated 35 mm glass bottom dishes, transfected at 70% confluency with equal amounts of plasmid DNA and used the next day. Ca^{2+} and cAMP imaging was performed at an inverted Leica TCS SP5 confocal laser-scanning microscope, (Leica DMI6000 B, Wetzlar, Germany) interfaced to a personal computer, running Leica Application Suite Advanced Fluorescence software (LAS AF 2.6). A 20X/0.7NA objective was used to acquire timelapse images (512 x 512 pixels with 1.2 s interval for live cell imaging). Cells were visualized via mCh or eGFP fluorescence with the 561 nm or 476 nm laser lines. Mouse melanopsin was activated and GCaMP6m was monitored with the 476 and 495 nm argon laser lines, whereas UVLamP was activated/deactivated and jRCaMP1b or Pink Flamindo was monitored with the 405 nm, 476 and 561 nm laser lines. The exact stimulation protocol is shown in the corresponding figure. The adenylyl cyclase activator Forskolin (Tocris, 100 µM) was bath applied at the last step of each stimulation. Fluorescence intensity of the respective sensor signal was measured over time for individual cells, normalized and scaled to the maximal response amplitude. Captured images were transferred into ImageJ software (1.47v; NIH) and analyzed with the time series analyzer V3 plugin.

In vitro electrophysiology

For GIRK channel recordings light sensitive GPCRs were expressed in HEK GIRK 1/2 cells (see above). Cells were cultured on 35 mm dishes and recorded in dark room conditions after transfection. GIRK-mediated K^+-currents were measured and analyzed as described in the following (see also [6]). The external solution was as follows: 20 mM NaCl, 120 mM KCl, 2 mM $CaCl_2$, 1 mM $MgCl_2$, 10 mM HEPES-KOH, pH 7.3 (KOH). Patch pipettes (2–5 MΩ) were filled with internal solution: 100 mM potassium aspartate, 40 mM KCl, 5 mM MgATP, 10 mM HEPES-KOH, 5 mM NaCl, 2 mM EGTA, 2 mM $MgCl_2$, 0.01 mM GTP, pH 7.3 (KOH). Cells were recorded in external solution containing 1µM 9-cis retinal (Sigma). The high affinity GIRK channel blocker Tertiapin-Q (Tocris, 1 µM) was bath applied while recording positive cells in whole-cell patch clamp configuration. Experiments were conducted with an inverted

microscope (Axiovert, ZEISS) and patch pipettes were controlled with a multi-micromanipulator (MPC-325, SUTTER INSTRUMENT). Transfected cells were visualized and UVLamP was manipulated with a monochromator system (Polychrome V, TILL Photonics). The stimulation protocols consisted of 100 ms, 360 nm, 0.7 mW/mm² light pulses for activation and 100 ms, 470 nm, 0.7 mW/mm² light pulses for deactivation if not stated otherwise in the corresponding figures. For the characterization of UVLamP wavelength dependence, light pulse duration dependence and intensity dependence, protocols were pseudorandomized and UVLamP was maximally deactivated between each trial. Whole-cell patch clamp recordings of HEK cells were performed, digitized at 10 kHz and filtered with an EPC10 USB amplifier (HEKA). Series resistances were partially compensated between 70 and 90%. The PatchMaster software (HEKA) was used for monochromator and voltage controls as well as data acquisition, and off-line analysis was made with Igor Pro 6.0 software (Wavemetrics).

Statistics

Statistical significance, test procedure and numbers of cells and/or trials performed (n) are specified in the figure legends. Statistical significance in all experiments was evaluated using SigmaPlot software (Systat Software) or Igor Pro software (WaveMetrics). For all results, the level of significance was set to $p < 0.05$. Statistical significance is indicated with *** $p < 0.001$; ** $p < 0.01$; * $p < 0.05$; n.s. (not significant).

Molecular mechanics simulations

The constructed model was prepared as starting structure for molecular mechanics (MM) simulations in the Moby program suite [7]. Structure preparation included dihedral-, angle-, and bond corrections according to the united atom Amber84 force field [8]. MM simulations were performed according to our previous publications [9,10]. We used the OPLS/AA all atom force field and GROMACS version (2019.3) [11]. All Systems were initially solvated following the Vedani-type [12] and thoroughly solvated in a cubic simulation cell with TIP4P water [13] and 154 mM NaCl. Membrane insertion was performed by using lambada [14] (to calculate a hydrophobic belt) and g_membed [14] (to embed the protein in the membrane).

Model construction software

The VMD [15] plugin QwikMD [16] was used to set up and conduct interactive molecular dynamics (iMD) simulations and molecular dynamics flexible fitting (MDFF) runs employing NAMD [17] with the CHARMM36 force field [18]. We also used Rosetta [19–21] for *ab initio* structure prediction. Modeller [22] was employed for homology modeling. A detailed description of the modeling workflow is given below under Model construction and Model validation.

Model construction strategy

We used our recently developed hybrid modeling workflow [10] to generate a structural model of the Japanese lamprey parapinopsin (GenBank accession number: AB116380.1). The key benefit of this concept is to streamline and facilitate the usage of *ab* inito structure prediction and homology modeling in combination with molecular dynamics simulations. The basis for the model is the bovine rhodopsin crystal structure (PDB-ID 1u19) [23]. The employed sequence alignment for homology modeling in shown in Figure S2. We incorporated additional information about helical regions, which we identified using *ab initio* structure prediction with Rosetta [19–21], structure prediction meta server like constrained consensus topology prediction server (CCTOP) [24] and the Bioinformatics Toolkit [25], as well as homology modeling server like Swiss Model [26] and Lomets [27]. All results are summarized in Figure S3 and the finally used secondary structure is highlighted in green within Figure S2. Conserved functional elements serve as anchor residues considered as residues in the helical region that are identical within a multiple sequence alignment marked with bold stars in Figure S2. For the multiple sequence alignment we used the Glucagon-like peptide1 receptor (PDB-ID 5VAI [28]), the Calcitonin receptor (PDB-ID 5UZ7 [29]), the Beta-2 adrenergic receptor (PDB-ID 3SN6 [30]), the Bos taurus Rhodopsin (PDB-ID 3DQB [31]), and the Squid rhodopsin (PDB-ID 2Z73 [32]).
The X-ray structure of the heterotrimeric G_i protein (PDB-ID 1gp2 [33]) from rat served as basis to construct human GDP bound $G\alpha_o$. As it was shown that the GDP bound state of $G\alpha_i$ has an

Mg^{2+} bound to GDP we added the Mg^{2+} including the three coordinating water molecules and replaced the side chain of Ser47 and the loop from residue number 176 to 183 including the Mg^{2+} coordinating Thr181 using the X-ray structure of the isolated Gα subunit with bound Mg^{2+} (PDB-ID 1bof [34]). Then, the resulting rat G_i protein with bound GDP and Mg^{2+} was used as template to build the homology model of human G_o protein employing SCWRL 4.0 [35]. The sequence alignments of all three G protein subunits are shown in Figures S4-6.
The complex with the G protein was constructed based on the β2AR crystal structure (PDB-ID 3SN6 [30]). The parapinopsin model was aligned with β2AR and our G protein model with the one of the X-ray structure. As helix 5 and 6 from parapinopsin clash with the Gα subunit we used QwikMD [16] to run an interactive molecular dynamics simulation using NAMD [17] through VMD [15] to move these two helices outwards. We assume that the overall shape between the β2AR and the G_s protein is highly similar to the shape of the parapinopsin G protein complex. Therefore, we refined the parapinopsin G protein complex to the shape of β2AR using molecular dynamics flexible fitting (MDFF) simulations [36]. The X-ray structure of β2AR (PDB-ID 3SN6 [30]) was converted into a volumetric density using volutiles of VMD [15]. QwikMD [16] was used to set up and conduct MDFF runs employing NAMD [17] with the CHARMM36 force field [18]. We constructed the melanopsin G_o protein complex following the same strategy as described for parapinopsin. We used the uncomplexed melanopsin model from Tennigkeit et al. [10] and the same GDP bound G protein as used for parapinopsin.
Within the iterative process that involves Monte Carlo based (Rosetta) [19–21] and MD based structure optimization (Moby-program package (H. Höweler, MAXIMOBY, CHEOPS, Altenberge, Germany, 2007)) the final model of parapinopsin in complex with human G_o is solvated, placed into the membrane and optimized regarding, side chain orientation, and hydrogen bond network. Then, the model is equilibrated by MM simulations (Gromacs 2019.3 [11]) to adapt to its physiological environment.

Model validation
Table S1 reflects a high sequence similarity of 70 % (identity 42 %) for the helical area of parapinopsin compared to bovine rhodopsin. A correct alignment is further ensured by the above described anchor residues. In addition, the key functional region, the retinal binding pocket, contains highly conserved functionally relevant amino acids. Based on these values we expect a highly accurate homology model of parapinopsin. The rat G_i and human G_o protein have an almost identical sequence (Figures S4-6), therefore, we also expect a highly reliable G protein model. Figure S7 shows the convergency to a stable plateau of the RMSD within our 475 ns MD simulations of the parapinopsin G_o protein complex and the melanopsin G_i protein complex. This convergency reflects that both simulation systems have reached a stable conformation.

Supplementary Table and Figures

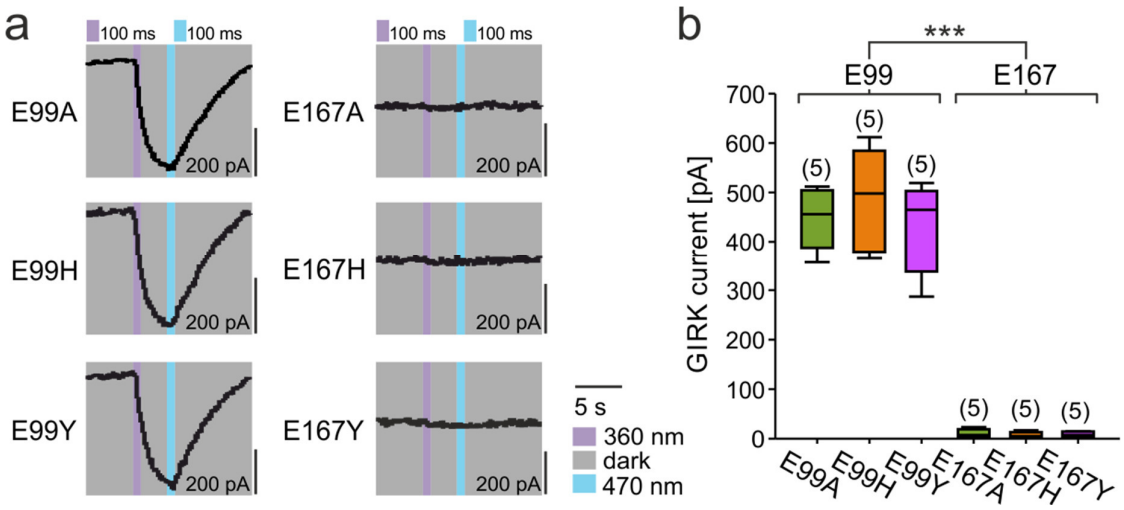

Figure S1. *In vitro* characterization of japanese lamprey parapinopsin ("UVLamP") counterion point mutations via whole-cell patch clamp recordings of GIRK currents in HEK GIRK 1/2 cells. a) Example traces of light induced induced GIRK currents for UVLamP E99A/H/Y and E167A/H/Y point mutants. b) Light induced GIRK currents for UVLamP E99A/H/Y and E167A/H/Y point mutants.

Table S1. Sequence identity and similarity of parapinopsin and bovine rhodopsin. Data are given in %.

%	All	No Ter	H1-8	H1	H2	H3	H4	H5	H6	H7	H8
Identity	39	41	42	23	43	46	33	35	56	60	55
Similarity	66	67	70	58	60	71	71	62	81	90	73

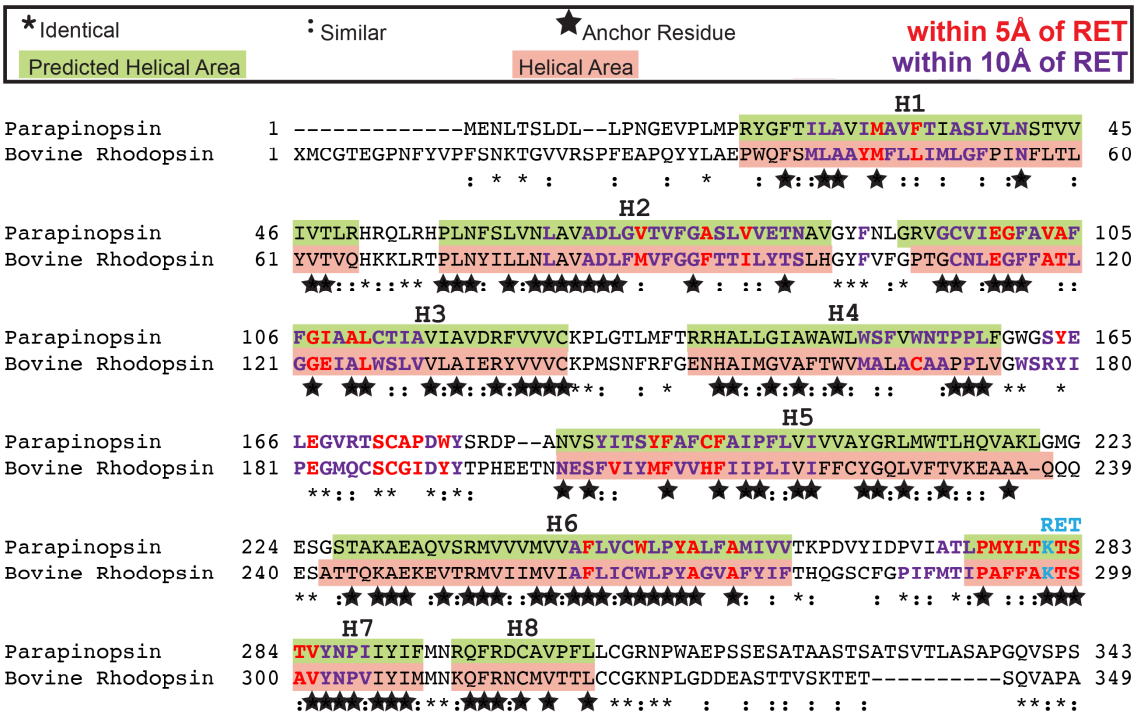

Figure S2. Parapinopsin model construction. Sequence alignment of parapinopsin with bovine rhodopsin [23]. The residues within 5 Å distance around the retinal are marked red and between 5 to 10 Å are purple. The predicted helices are highlighted in green and the helical residues of the X-ray structures in light red.

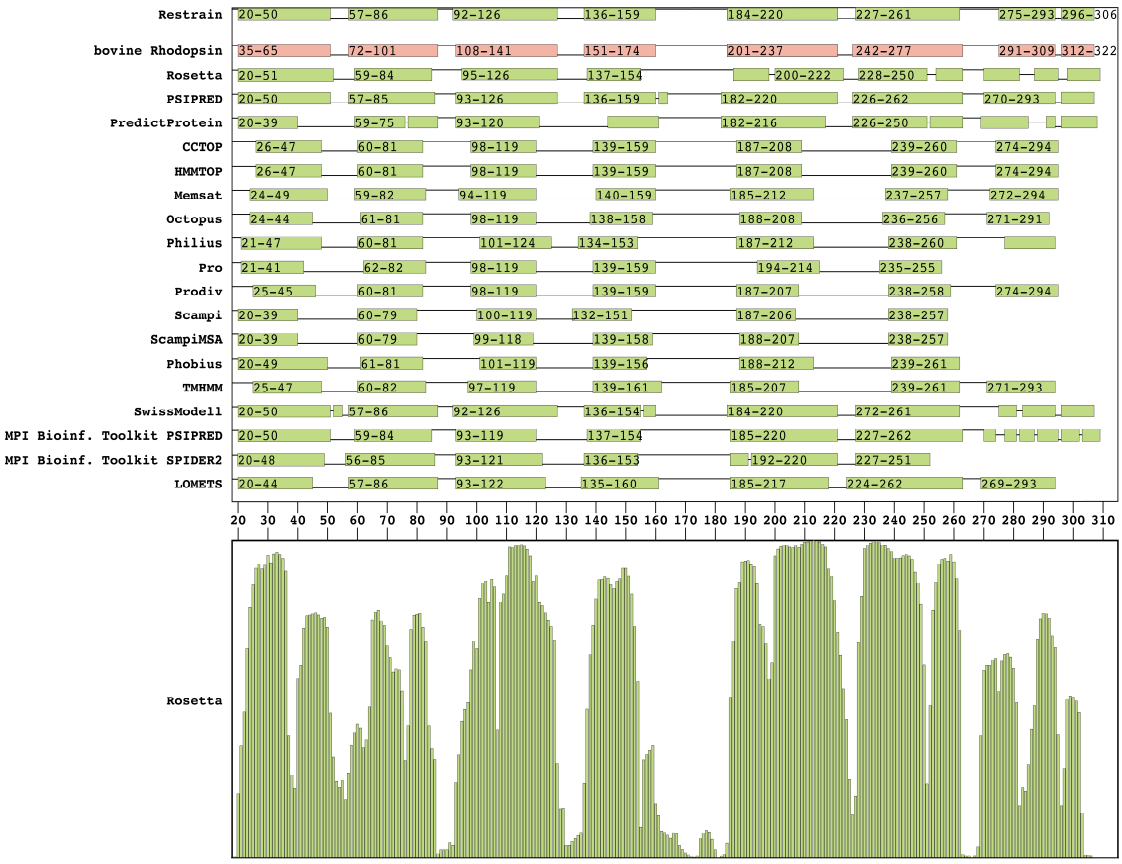

Figure S3. Secondary structure prediction of parapinopsin. The top illustrates the secondary structure prediction results for parapinopsin and the bottom represents the results of the rosetta secondary structure prediction for the same template. All results were merged and included as restrains in the calculation of the homology model. The helical area of the bovine rhodopsin crystal structure (PDB-ID 1u19 [23]) is colored in light red.

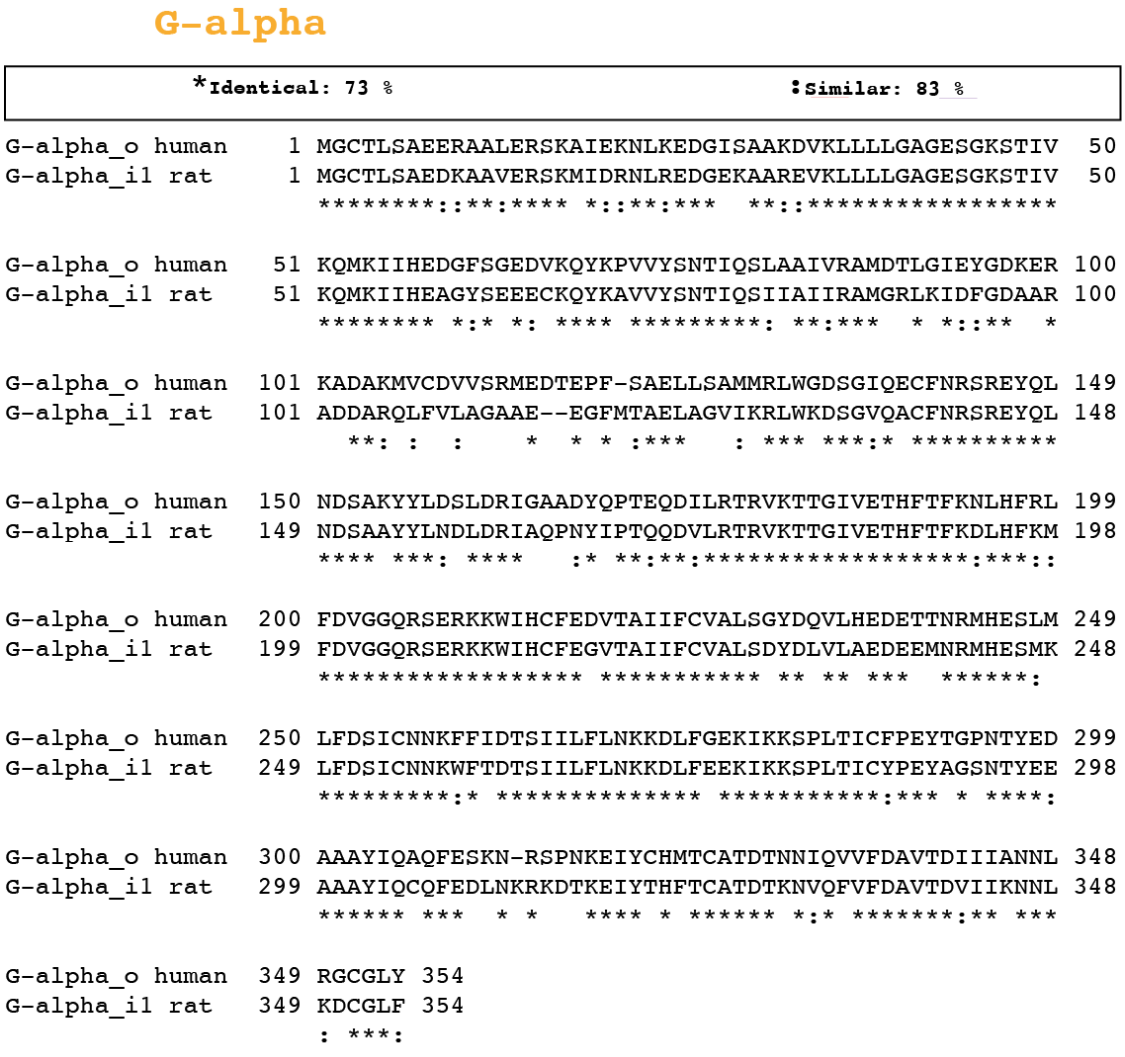

Figure S4. Sequence alignment of $G\alpha_{i/o}$. Shown is the sequence alignment between $G\alpha_i$ rat (PDB-ID: 1GP2 [33])and $G\alpha_o$ human (UNIPROT-ID: P09471).

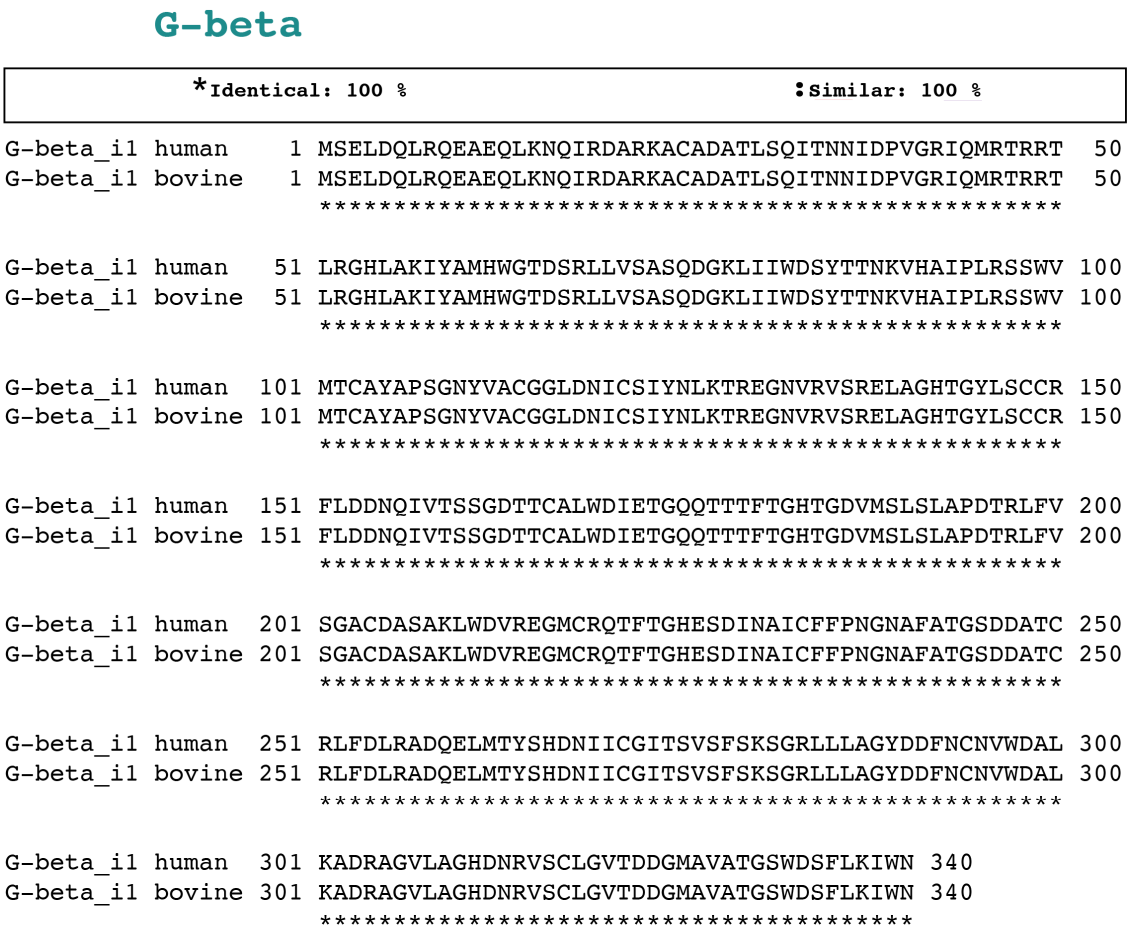

Figure S5. Sequence alignment of Gβ. Shown is the sequence alignment between Gβ1 bovine (PDB-ID 1GP2 [33]) and Gβ1 human (UNIPROT-ID: P62873).

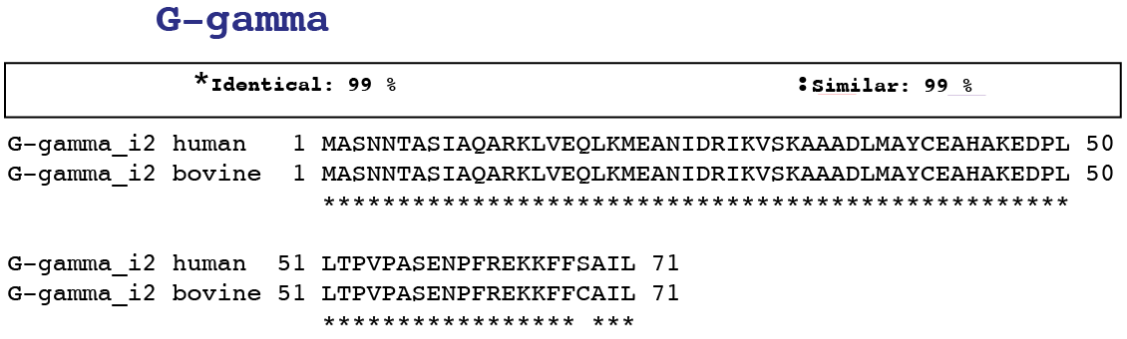

Figure S6. Sequence alignment of Gγ. The sequence alignment between Gγ2 bovine (PDB-ID 1GP2 [33]) and Gγ2 human (UNIPROT-ID: P59768) is represented.

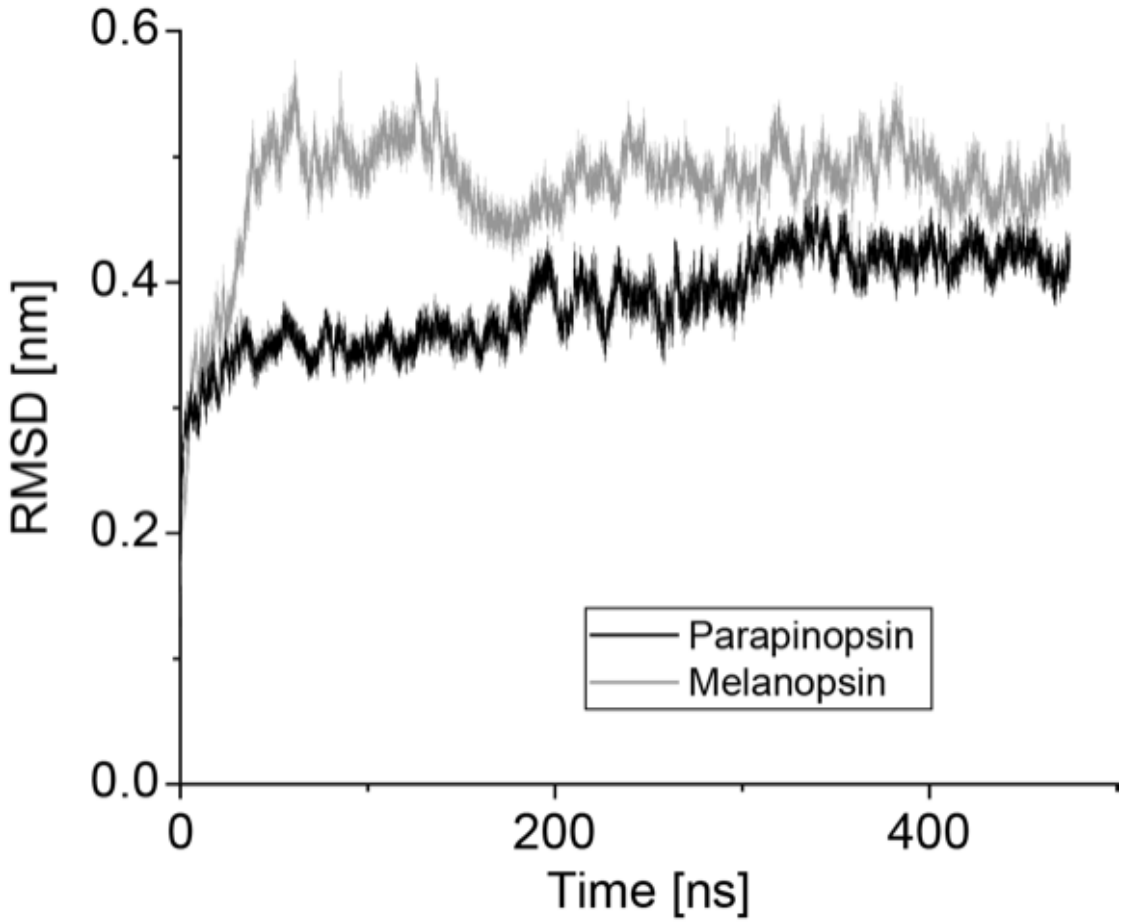

Figure S7. RMSD of the MM simulations based on our constructed models. Shown is the RMSD of the Cα-atoms of the equilibration MM simulations for parapinopsin (black) and melanopsin (light gray). All illustrated RMSDs are stable.

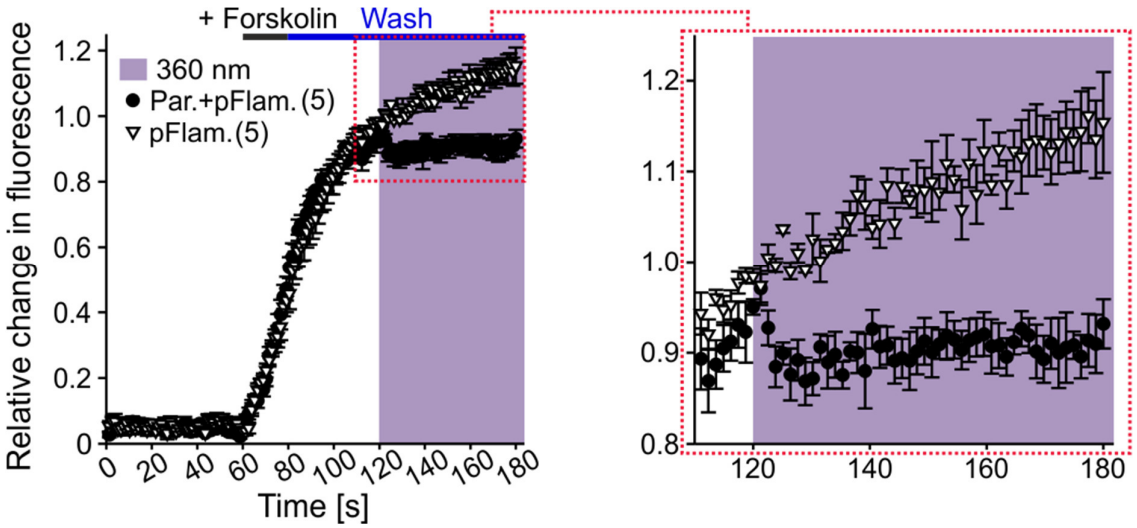

Figure S8. Light induced blockage of Gs mediated intracellular cAMP increase in HEK tsA201 cells for UVLamP (UVLaMP + Pink Flamindo) vs. Control (Pink Flamindo). Cells were stimulated with Forskolin/UV light and compound was washed out as indicated.

References

[1] J.-H. Choi, N.-K. Yu, G.-C. Baek, J. Bakes, D. Seo, H. J. Nam, S. H. Baek, C.-S. Lim, Y.-S. Lee, B.-K. Kaang, *Mol. Brain* **2014**, *7*, 17.

[2] a) A. Terakita, M. Koyanagi, H. Tsukamoto, T. Yamashita, T. Miyata, Y. Shichida, *Nat. Struct. Mol. Biol.* **2004**, *11*, 284; b) M. Koyanagi, E. Kawano, Y. Kinugawa, T. Oishi, Y. Shichida, S. Tamotsu, A. Terakita, *PNAS* **2004**, *101*, 6687.

[3] H. M. Beyer, P. Gonschorek, S. L. Samodelov, M. Meier, W. Weber, M. D. Zurbriggen, *PLoS One* **2015**, *10*, e0137652.

[4] K. Spoida, D. Eickelbeck, R. Karapinar, T. Eckhardt, M. D. Mark, D. Jancke, B. V. Ehinger, P. König, D. Dalkara, S. Herlitze et al., *Curr. Biol.* **2016**, *26*, 1206.

[5] a) T.-W. Chen, T. J. Wardill, Y. Sun, S. R. Pulver, S. L. Renninger, A. Baohan, E. R. Schreiter, R. A. Kerr, M. B. Orger, V. Jayaraman et al., *Nature* **2013**, *499*, 295; b) H. Dana, B. Mohar, Y. Sun, S. Narayan, A. Gordus, J. P. Hasseman, G. Tsegaye, G. T. Holt, A. Hu, D. Walpita et al., *eLife* **2016**, *5*; c) K. Harada, M. Ito, X. Wang, M. Tanaka, D. Wongso, A. Konno, H. Hirai, H. Hirase, T. Tsuboi, T. Kitaguchi, *Sci. Rep.* **2017**, *7*, 7351.

[6] X. Li, D. V. Gutierrez, M. G. Hanson, J. Han, M. D. Mark, H. Chiel, P. Hegemann, L. T. Landmesser, S. Herlitze, *PNAS* **2005**, *102*, 17816.

[7] U. Höweler, *MAXIMOBY, CHEOPS, Altenberge, Germany*, **2007**.

[8] L. Yang, Å. A. Skjevik, W.-G. Han Du, L. Noodleman, R. C. Walker, A. W. Götz, *Data Brief* **2016**, *8*, 1209.

[9] a) K. Eisenhauer, J. Kuhne, E. Ritter, A. Berndt, S. Wolf, E. Freier, F. Bartl, P. Hegemann, K. Gerwert, *J. Biol. Chem.* **2012**, *287*, 6904; b) J. Kuhne, K. Eisenhauer, E. Ritter, P. Hegemann, K. Gerwert, F. Bartl, *Angew. Chem., Int. Ed. Engl.* **2015**, *54*, 4953; c) J. Kuhne, J. Vierock, S. A. Tennigkeit, M.-A. Dreier, J. Wietek, D. Petersen, K. Gavriljuk, S. F. El-Mashtoly, P. Hegemann, K. Gerwert, *PNAS* **2019**, *116*, 9380.

[10] S. A. Tennigkeit, R. Karapinar, T. Rudack, M.-A. Dreier, P. Althoff, D. Eickelbeck, T. Surdin, M. Grömmke, M. D. Mark, K. Spoida et al., *ChemBioChem* **2019**, *20*, 1766.

[11] M. J. Abraham, T. Murtola, R. Schulz, S. Páll, J. C. Smith, B. Hess, E. Lindahl, *SoftwareX* **2015**, *1-2*, 19.

[12] A. Vedani, D. W. Huhta, *J. Am. Chem. Soc.* **1991**, *113*, 5860.

[13] a) W. L. Jorgensen, J. Chandrasekhar, J. D. Madura, R. W. Impey, M. L. Klein, *J. Chem. Phys.* **1983**, *79*, 926; b) H. W. Horn, W. C. Swope, J. W. Pitera, J. D. Madura, T. J. Dick, G. L. Hura, T. Head-Gordon, *J. Chem. Phys.* **2004**, *120*, 9665.

[14] T. H. Schmidt, C. Kandt, *J. Chem. Inf. Model.* **2012**, *52*, 2657.

[15] W. Humphrey, A. Dalke, K. Schulten, *J. Mol. Graphics* **1996**, *14*, 33.

[16] J. V. Ribeiro, R. C. Bernardi, T. Rudack, J. E. Stone, J. C. Phillips, P. L. Freddolino, K. Schulten, *Sci. Rep.* **2016**, *6*, 26536.

[17] J. C. Phillips, R. Braun, W. Wang, J. Gumbart, E. Tajkhorshid, E. Villa, C. Chipot, R. D. Skeel, L. Kalé, K. Schulten, *J. Comput. Chem.* **2005**, *26*, 1781.

[18] J. Huang, A. D. MacKerell, *J. Comput. Chem.* **2013**, *34*, 2135.

[19] A. Leaver-Fay, M. Tyka, S. M. Lewis, O. F. Lange, J. Thompson, R. Jacak, K. Kaufman, P. D. Renfrew, C. A. Smith, W. Sheffler et al., *Methods Enzymol.* **2011**, *487*, 545.

[20] K. W. Kaufmann, G. H. Lemmon, S. L. Deluca, J. H. Sheehan, J. Meiler, *Biochemistry* **2010**, *49*, 2987.

[21] S. Lindert, J. A. McCammon, *J. Chem. Theory Comput.* **2015**, *11*, 1337.

[22] A. Sali, T. L. Blundell, *J. Mol. Biol.* **1993**, *234*, 779.

[23] T. Okada, M. Sugihara, A.-N. Bondar, M. Elstner, P. Entel, V. Buss, *J. Mol. Biol.* **2004**, *342*, 571.

[24] M. Stemmer, T. Thumberger, M. Del Sol Keyer, J. Wittbrodt, J. L. Mateo, *PLoS One* **2015**, *10*, e0124633.

[25] L. Zimmermann, A. Stephens, S.-Z. Nam, D. Rau, J. Kübler, M. Lozajic, F. Gabler, J. Söding, A. N. Lupas, V. Alva, *J. Mol. Biol.* **2018**, *430*, 2237.

[26] T. Schwede, J. Kopp, N. Guex, M. C. Peitsch, *Nucleic Acids Res.* **2003**, *31*, 3381.

[27] S. Wu, Y. Zhang, *Nucleic Acids Res.* **2007**, *35*, 3375.

[28] Y. Zhang, B. Sun, D. Feng, H. Hu, M. Chu, Q. Qu, J. T. Tarrasch, S. Li, T. Sun Kobilka, B. K. Kobilka et al., *Nature* **2017**, *546*, 248.
[29] Y.-L. Liang, M. Khoshouei, M. Radjainia, Y. Zhang, A. Glukhova, J. Tarrasch, D. M. Thal, S. G. B. Furness, G. Christopoulos, T. Coudrat et al., *Nature* **2017**, *546*, 118.
[30] S. G. F. Rasmussen, B. T. DeVree, Y. Zou, A. C. Kruse, K. Y. Chung, T. S. Kobilka, F. S. Thian, P. S. Chae, E. Pardon, D. Calinski et al., *Nature* **2011**, *477*, 549.
[31] P. Scheerer, J. H. Park, P. W. Hildebrand, Y. J. Kim, N. Krauss, H.-W. Choe, K. P. Hofmann, O. P. Ernst, *Nature* **2008**, *455*, 497.
[32] M. Murakami, T. Kouyama, *Nature* **2008**, *453*, 363.
[33] M. A. Wall, D. E. Coleman, E. Lee, J. A. Iñiguez-Lluhi, B. A. Posner, A. G. Gilman, S. R. Sprang, *Cell* **1995**, *83*, 1047.
[34] D. E. Coleman, S. R. Sprang, *Biochemistry* **1998**, *37*, 14376.
[35] G. G. Krivov, M. V. Shapovalov, R. L. Dunbrack, *Proteins* **2009**, *77*, 778.
[36] L. G. Trabuco, E. Villa, K. Mitra, J. Frank, K. Schulten, *Structure* **2008**, *16*, 673.

Author contributions

D.E., R.K., S.A.T., T.R. and S.H. conceived and analyzed experiments. T.S. and R.K. generated plasmid constructs. D.E., R.K., J.S. and B.M. performed cell culture assays. D.E. conducted cell culture electrophysiology experiments. S.A.T. and T.R., together with M.Sh., M.Sc. and P.A., performed biophysical modelling experiments and created the modelling figures. D.E. designed the figures and wrote the manuscript with input and detailed descriptions from all authors for their specific contributions.